Preprint version of: J. Carbajo, A. Prieto, J. Ramis, L. Río-Martín, A non-parametric fluid-equivalent approach for the acoustic characterization of rigid porous materials, Applied Mathematical Modelling, Volume 76, 2019,Pages 330-347, https://doi.org/10.1016/j.apm.2019.05.046.

Acoustic characterization of rigid porous materials by using non-parametric fluid-equivalent models

J. Carbajo[a], A. Prieto[b,*], J. Ramis[c], L. Río-Martín[b]

[a] *University of Alicante, Department of Civil Engineering, 03080, San Vicente del Raspeig, Spain*
[b] *University of Alicante, Department of Physics, System Engineering and Signal Theory, 03080, San Vicente del Raspeig, Spain*
[c] *University of A Coruña, Department of Mathematics, 15071, A Coruña, Spain*

Abstract

The acoustic characterization of porous materials with rigid solid frame plays a key role in the prediction of the acoustic behaviour of any dynamic system that incorporates them. In order to obtain an accurate prediction of its frequency-dependent response, a suitable choice of the parametric models for each material is essential. However, such models could be inadequate for a given material or only valid in a specific frequency range. In this work, a novel non-parametric methodology is proposed for the characterization of the acoustic properties of rigid porous materials. This technique is based on the solution of a sequence of frequency-by-frequency well-posed inverse problems. Once a reduced number of experimental measurements are available, the proposed method avoids the *a priori* choice of a parametric model.

Keywords: Material characterization, Porous materials, Inverse problem
2010 MSC: 74D05, 70J10, 74J25

1. Introduction

Rigid porous materials are widely used for noise mitigation in a large number of engineering applications in building and environmental acoustics. In this

*Corresponding author
Email addresses: jesus.carbajo@ua.es (J. Carbajo), andres.prieto@udc.es (A. Prieto), jramis@ua.es (J. Ramis), laura.rmartin@udc.es (L. Río-Martín)

context, it is of great interest to predict the acoustic properties of these materials when they are being part of noise control devices (e.g. noise barriers [1], isolation walls [2]...). Usually, the porous material is modelled in a macroscopic scale as an equivalent fluid having frequency-dependent complex acoustic properties, namely, characteristic impedance and wave number [3]. These acoustic properties can be easily determined using a parametric prediction model (e. g. [4, 5]) from the intrinsic physical properties of the material (e.g. flow resistivity, porosity...), these latter being measured following laboratory procedures.

In general, these parametric models are based on the asymptotic behaviour at low and high frequencies of rigid porous media [4, 5] or make use of empirical relations [6] to describe the sound propagation through the material. In any case, it is necessary to determine one or several of its intrinsic physical properties prior to deriving its acoustic properties. While there exist several experimental methods and techniques [7] that let determine these physical parameters, a common alternative to these procedures consists in using a derivative-free optimization procedure [8] to fit the values of these properties. In brief, an inverse methodology can be employed to minimize the difference between the measured acoustic properties and those calculated using a prediction model whose parameters need to be fitted. In most cases, and so as to simplify the fitting procedure, a wide-band frequency spectrum of the surface impedance or the sound absorption coefficient are used for this adjustment [9–11]. Both the surface impedance and the sound absorption coefficient can be obtained for a given material when it is used as a sound absorber (i.e.layer of porous material backed by a rigid wall). The main drawback of this parametric methodology is that these minimization procedures require using multiple frequency values for the adjustment, which may constrain the solution of the inverse problem given by a specific parametric model. Moreover, the chosen parametric model could be not suitable for a particular material (e.g., the use of a single-parameter model [6] may not be accurate enough to properly describe the acoustic behaviour of a rigid porous material). In fact, although many parametric models exist in the literature [3–6, 12], the incessant development of new materials poses the need

for alternative predictive tools and fitting methods.

In this work, a novel non-parametric methodology for the characterization of rigid porous materials is proposed. Unlike the above approaches, the proposed procedure avoids any parametric assumption or the need to determine intrinsic physical parameters using sophisticated laboratory equipment. Instead, this non-parametric methodology uses traditional two-microphone impedance tube setup [13] data to solve a fixed-frequency propagation problem and thus estimate the acoustic properties of the material under study. Even though there exist other methods based on impedance tube arrangements for measuring the acoustic properties of porous materials [14–16], most of them require complementary appliances or more complex equipment configurations. On one hand, since the proposed non-parametric methodology does not depend on the physical nature of the material itself, it is expected to be more generic than the traditional predictive parametric approaches and may be applied to any type of porous material (i.e., fibrous, granular,...).

On the other hand, the use of multilayered or stratified media is great interest in real-life engineering applications (from a thermal [17] and an acoustic [18] point of view). So, the proposed methodology was found to be extensible to the analysis of multilayered systems containing light porous layers, which is of great interest because of the laboratory difficulties associated with the accurate characterization of the latter alone using an impedance tube. In order to validate the proposed non-parametric approach, different sets of experimental data based on single and multilayer configurations were compared with respect to the numerically fitted results, a good agreement being found in both cases. Therefore, this novel numerical methodology may be regarded as a simple and straightforward alternative for the characterization of rigid porous materials, to be used in the design stage thereof. In addition, in order to write the acoustic propagation problems using an uniform approach valid for different multilayer configurations, the inverse problems stated throughtout this work have been stated in terms of the surface admittance values (instead using the classical surface impedance values [2, 3, 14]).

This paper is organized as follows: Section 2 describes the acoustic quantities used to characterize rigid porous materials as well as the experimental setup used to measure these, along with the mathematical statement of the inherent propagation problem. In Section 3, the inverse problem methodology used to obtain the acoustic properties of a rigidly backed single porous layer is described in detail. Four different strategies are outlined, each of them successively overcoming the limitations of the traditional fitting procedures used for the same purpose. Section 4 presents an extension of that methodology but for the case of a double porous layer configuration. In Section 5, the numerical procedure followed to solve the well-posed inverse problems is described. Section 6 presents the numerical results obtained, both for the single and double layer configurations, showing a good agreement when compared to measured data. Finally, Section 7 summarizes the main conclusions of this work.

Remark 1.1. *Throughout this manuscript, time-harmonic dependence for the acoustic pressure and displacement fields will be assumed. In this manner, it has been settled formally that* $\pi(\boldsymbol{x},t) = \mathrm{Re}(\Pi(\boldsymbol{x})e^{j\omega t})$*, being* π *the time-dependent acoustic pressure field,* Π *the complex-valued time-harmonic acoustic pressure field,* ω *the angular frequency,* t *the time variable,* $\boldsymbol{x}$ *the Cartesian coordinates of the spatial position,* $\mathrm{Re}(\cdot)$ *the real part function of a complex number, and* $j = \sqrt{-1}$ *the imaginary unit.*

2. Harmonic response of a rigid porous material

2.1. Macroscopic description

Linear theory regarding the propagation of sound in air-saturated rigid porous media has been extensively studied in the last decades (see, for instance, [3]). Basically, rigid porous materials attenuate sound mainly due to viscous friction and thermal conductivity in their pore network. If the pore size is small compared to the wavelength of an impinging sound wave, the air inside a layer of porous material with rigid solid frame (i.e., motionless skeleton) can be modeled accurately on a macroscopic scale as an equivalent compressible fluid. The

acoustical behavior of the material is then fully characterized by the complex-valued and frequency-dependent dynamic coefficient pair: dynamic mass density $\rho_{\mathrm{P}}(\omega)$ and dynamic bulk modulus $K_{\mathrm{P}}(\omega)$. Alternatively, the acoustic response of this fluid-equivalent model can be determined from the coefficient pair: dynamic characteristic impedance, $Z_{\mathrm{P}}(\omega)$, and wave number, $k_{\mathrm{P}}(\omega)$, which are so-called intrinsic acoustic properties, these being related to the previous ones by

$$Z_{\mathrm{P}}(\omega) = \sqrt{\rho_{\mathrm{P}}(\omega) K_{\mathrm{P}}(\omega)}, \tag{1}$$

$$k_{\mathrm{P}}(\omega) = \omega \sqrt{\rho_{\mathrm{P}}(\omega) / K_{\mathrm{P}}(\omega)}. \tag{2}$$

2.2. Experimental characterization

Experimental methods frequently used for the acoustic characterization of porous materials use an impedance tube arrangement [14–16]. Particularly, Utsuno et al. [14] proposed the experimental setup shown in Figure 1 to estimate the acoustic properties of a single porous layer configuration. In brief, a source (typically an audio speaker) generates plane waves that impinge on the porous material positioned on the other end of the tube. The characteristic impedance (1) and the wave number (2) of the material under test are determined by using the pressure data from a pair of microphones flush mounted in the tube for two porous sample configurations: rigid-backed and air-cavity backed.

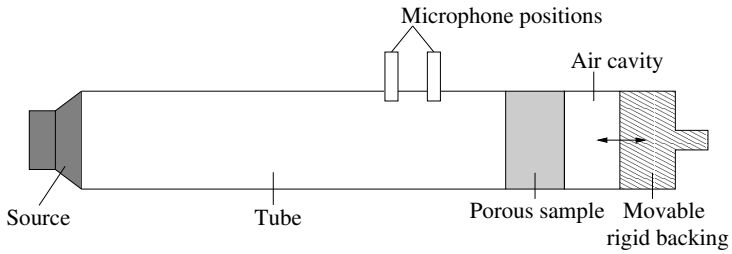

Figure 1: Impedance tube setup proposed by Utsuno et al. [14] to determine the characteristic impedance and wave number of porous materials in a single layer configuration.

Once the acoustic properties that characterize a rigid porous material and the experimental method used to measure these were outlined, a description of

the mathematical model that let us solve the associated inverse problem and subsequently the inherent direct propagation problem is given.

2.3. Statement of the direct propagation problem

When the porous medium with rigid solid frame is assumed to be homogeneous and isotropic on a macroscopic scale, its intrinsic acoustic properties are considered spatially constant, and so the classical Helmholtz and momentum equations describing the acoustic wave propagation in such medium (written in terms of the corresponding pair of coefficients $\rho_{\mathrm{P}}(\omega)$ and $k_{\mathrm{P}}(\omega)$) are given by

$$-k_{\mathrm{P}}^2(\omega)\Pi_{\mathrm{P}} - \Delta\Pi_{\mathrm{P}} = 0, \tag{3}$$

$$-\omega^2\rho_{\mathrm{P}}(\omega)\boldsymbol{U}_{\mathrm{P}} - \nabla\Pi_{\mathrm{P}} = \mathbf{0}, \tag{4}$$

where Π_{P} and $\boldsymbol{U}_{\mathrm{P}}$ are the acoustic pressure and displacement fields in the porous medium, respectively.

In order to model mathematically the acoustic wave propagation throughout a rigid-backed porous layer placed inside an impedance tube, a multilayer planar configuration formed by a porous layer surrounded by a compressible fluid in the front face is considered. To write the strong differential formulation of the coupled problem, both the compressible fluid model and the porous models have been written in terms of the pressure field. Let Ω_{F} and Ω_{P} be the three-dimensional domains occupied by the fluid and the porous layer, respectively (see Figure 2). The fluid is placed in the interior of a tube with constant cross section and the thickness of the porous sample is finite (denoted by d). The coupled interface Γ_{I} denotes the common boundary between the fluid and the porous layer. The lateral rigid wall of the tube is denoted by Γ_{W}. The boundary Γ_{L} is the location where the acoustic source (audio speaker) is placed. The back boundary of the porous layer is denoted by Γ_{B} For a better understanding of the notation, Figure 2 shows a two-dimensional cut of the computational domain where the boundaries and the fluid and porous subdomains are depicted.

Since the acoustic behavior of a rigid-frame porous material could be represented by an fluid-equivalent model (3)-(4), then the strong differential formu-

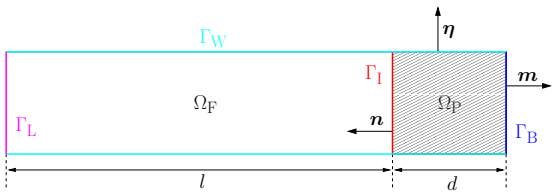

Figure 2: Schematic two-dimensional cut of the impedance tube where the fluid and the porous subdomains, Ω_F and Ω_P, are marked in white and dashed regions, respectively. Their boundaries are highlighted with different colors: Γ_I in red, Γ_W in cyan, Γ_L in magenta, and Γ_B in blue.

lation for this coupled problem is given by: for a fixed angular frequency $\omega > 0$, a prescribed back surface admittance operator Y_B, and an acoustic loudspeaker source G, find the fluid pressure and displacement fields, Π_F and $\boldsymbol{U}_F$, and the porous pressure and displacement fields, Π_P and $\boldsymbol{U}_F$, such that

$$
\begin{cases}
-k_F^2(\omega)\Pi_F - \Delta\Pi_F = 0 & \text{in } \Omega_F, \\
-\omega^2\rho_F\boldsymbol{U}_F - \nabla\Pi_F = \boldsymbol{0} & \text{in } \Omega_F, \\
-k_P^2(\omega)\Pi_P - \Delta\Pi_P = 0 & \text{in } \Omega_P, \\
-\omega^2\rho_P(\omega)\boldsymbol{U}_P - \nabla\Pi_P = \boldsymbol{0} & \text{in } \Omega_P, \\
\boldsymbol{U}_F \cdot \boldsymbol{n} = \boldsymbol{U}_P \cdot \boldsymbol{n} & \text{on } \Gamma_I, \\
\Pi_F = \Pi_P & \text{on } \Gamma_I, \\
j\omega\boldsymbol{U}_P \cdot \boldsymbol{m} = Y_B\Pi_P & \text{on } \Gamma_B, \\
\boldsymbol{U}_F \cdot \boldsymbol{\eta} = 0 & \text{on } \Gamma_W \cap \partial\Omega_F, \\
\boldsymbol{U}_P \cdot \boldsymbol{\eta} = 0 & \text{on } \Gamma_W \cap \partial\Omega_P, \\
\Pi_F = G & \text{on } \Gamma_L,
\end{cases}
$$

where $k_F(\omega) = \omega/c_F$, being c_F the sound velocity and ρ_F the mass density in the fluid. Finally, $\boldsymbol{n}$, $\boldsymbol{m}$, and $\boldsymbol{\eta}$ are respectively the unit normal vectors on boundaries Γ_I, Γ_B, and Γ_W. These normal vectors are outward to the porous domain (on those boundaries where it is applicable).

Equivalently, the coupled problem stated above can be reformulated only in

terms of the fluid pressure field Π_{F} and the porous pressure field Π_{P}:

$$\begin{cases} -k_{\mathrm{F}}^2(\omega)\Pi_{\mathrm{F}} - \Delta\Pi_{\mathrm{F}} = 0 & \text{in } \Omega_{\mathrm{F}}, \\ -k_{\mathrm{P}}^2(\omega)\Pi_{\mathrm{P}} - \Delta\Pi_{\mathrm{P}} = 0 & \text{in } \Omega_{\mathrm{P}}, \\ \dfrac{1}{\rho_{\mathrm{F}}}\dfrac{\partial\Pi_{\mathrm{F}}}{\partial\boldsymbol{n}} = \dfrac{1}{\rho_{\mathrm{P}}(\omega)}\dfrac{\partial\Pi_{\mathrm{P}}}{\partial\boldsymbol{n}} & \text{on } \Gamma_{\mathrm{I}}, \\ \Pi_{\mathrm{F}} = \Pi_{\mathrm{P}} & \text{on } \Gamma_{\mathrm{I}}, \\ \dfrac{1}{j\omega\rho_{\mathrm{P}}(\omega)}\dfrac{\partial\Pi_{\mathrm{P}}}{\partial\boldsymbol{m}} = Y_{\mathrm{B}}\Pi_{\mathrm{P}} & \text{on } \Gamma_{\mathrm{B}}, \\ \dfrac{\partial\Pi_{\mathrm{F}}}{\partial\boldsymbol{\eta}} = 0 & \text{on } \Gamma_{\mathrm{W}} \cap \partial\Omega_{\mathrm{F}}, \\ \dfrac{\partial\Pi_{\mathrm{P}}}{\partial\boldsymbol{\eta}} = 0 & \text{on } \Gamma_{\mathrm{W}} \cap \partial\Omega_{\mathrm{P}}, \\ \Pi_{\mathrm{F}} = G & \text{on } \Gamma_{\mathrm{L}}. \end{cases} \tag{5}$$

Following standard arguments to model waveguides [19], it is assumed that the transversal section $\mathcal{S}$ of the impedance tube remains constant along its axis (in the x_1-direction), the loudspeaker is placed on plane $x_1 = -l$, and the coupling interface and the back surface are placed on planes $x_1 = 0$ and $x_1 = d$, respectively. Hence, $\Omega_{\mathrm{F}} = (-l, 0) \times \mathcal{S}$ and $\Omega_{\mathrm{P}} = (0, d) \times \mathcal{S}$ and then the $\mathrm{L}^2(S)$-Hilbert basis $\{\varphi_n\}_{n\in\mathbb{N}}$ of transverse modes associated to the impedance tube [20] can be computed as the eigenmodes of the two-dimensional problem on the $x_2 - x_3$ coordinate plane

$$\begin{cases} -\lambda_n^2\varphi_n - \dfrac{\mathrm{d}^2\varphi_n}{\mathrm{d}x_2^2} - \dfrac{\mathrm{d}^2\varphi_n}{\mathrm{d}x_3^2} = 0 & \text{in } \mathcal{S}, \\ \dfrac{\partial\varphi_n}{\partial\boldsymbol{r}} = 0 & \text{on } \partial\mathcal{S}, \end{cases}$$

where λ_n is the transverse eigenvalue associated to the n-th φ_n mode, and $\boldsymbol{r}$ denotes the unit normal vector on boundary $\partial\mathcal{S}$ exterior to $\mathcal{S}$. Since the coupling boundary Γ_{I} and the back surface Γ_{B} are assumed planar and placed on $x_1 = 0$ and $x_1 = d$, respectively, then the unit outward normal vectors are given by $\boldsymbol{n} = -\boldsymbol{e}_1$ and $\boldsymbol{m} = \boldsymbol{e}_1$, being $\{\boldsymbol{e}_1, \boldsymbol{e}_2, \boldsymbol{e}_3\}$ the canonical vector basis of the Cartesian system. Hence, the solution of the pressure fields (written in

Cartesian coordinates $\boldsymbol{x} = (x_1, x_2, x_3)$) are given by

$$\Pi_{\mathrm{F}}(\boldsymbol{x}) = \sum_{n=0}^{\infty} \left(a_{\mathrm{F}}^n e^{-j\beta_{\mathrm{F}}^n(\omega)x_1} + b_{\mathrm{F}}^n e^{j\beta_{\mathrm{F}}^n(\omega)x_1} \right) \varphi_n(x_2, x_3) \quad \text{for } \boldsymbol{x} \in \Omega_{\mathrm{F}}, \tag{6}$$

$$\Pi_{\mathrm{P}}(\boldsymbol{x}) = \sum_{n=0}^{\infty} \left(a_{\mathrm{P}}^n e^{-j\beta_{\mathrm{P}}^n(\omega)x_1} + b_{\mathrm{P}}^n e^{j\beta_{\mathrm{P}}^n(\omega)x_1} \right) \varphi_n(x_2, x_3) \quad \text{for } \boldsymbol{x} \in \Omega_{\mathrm{P}}, \tag{7}$$

where a_{F}^n, b_{F}^n, a_{P}^n, b_{P}^n are the modal coefficients associated to n-th mode for the fluid and porous pressure, respectively; $\beta_{\mathrm{F}}^n(\omega) = \sqrt{k_{\mathrm{F}}^2(\omega) - \lambda_n^2}$ and $\beta_{\mathrm{P}}^n(\omega) = \sqrt{k_{\mathrm{P}}^2(\omega) - \lambda_n^2}$ for $n \in \mathbb{N}$ (notice that the square root is computed with the positive criterion $\mathrm{Re}(\sqrt{z}) \geq 0$).

In addition, the pressure induced by the active boundary of the loudspeaker, Γ_{L}, can be represented by $G = \sum_{n=0}^{\infty} g_n \varphi_n$, and the action of the surface admittance operator Y_{B}, which can be read as a Dirichlet-to-Neumann (DtN) operator on Γ_{B} associated to problem (5) (see for instance [21, 22]), can be expressed by

$$F = \sum_{n=0}^{\infty} f_n \varphi_n \mapsto Y_{\mathrm{B}} F = \sum_{n=0}^{\infty} Y_{\mathrm{B}}^n(\omega) f_n \varphi_n.$$

Consequently, problem (5) can be decoupled in terms of the transverse modes, and hence the modal coefficients $\{a_{\mathrm{F}}^n, b_{\mathrm{F}}^n, a_{\mathrm{P}}^n, b_{\mathrm{P}}^n\}_{n\in\mathbb{N}}$ are solution of the following sequence of linear algebraic system of equations:

$$\begin{cases} \rho_{\mathrm{P}}(\omega)\beta_{\mathrm{F}}^n(\omega)(-a_{\mathrm{F}}^n + b_{\mathrm{F}}^n) = \rho_{\mathrm{F}}\beta_{\mathrm{P}}^n(\omega)(-a_{\mathrm{P}}^n + b_{\mathrm{P}}^n), \\ a_{\mathrm{F}}^n + b_{\mathrm{F}}^n = a_{\mathrm{P}}^n + b_{\mathrm{P}}^n, \\ \dfrac{\beta_{\mathrm{P}}^n(\omega)}{\omega\rho_{\mathrm{P}}(\omega)} \left(-a_{\mathrm{P}}^n e^{-j\beta_{\mathrm{P}}^n(\omega)d} + b_{\mathrm{P}}^n e^{j\beta_{\mathrm{P}}^n(\omega)d} \right) = Y_{\mathrm{B}}^n(\omega) \left(a_{\mathrm{P}}^n e^{-j\beta_{\mathrm{P}}^n(\omega)d} + b_{\mathrm{P}}^n e^{j\beta_{\mathrm{P}}^n(\omega)d} \right), \\ a_{\mathrm{F}}^n e^{j\beta_{\mathrm{F}}^n(\omega)l} + b_{\mathrm{F}}^n e^{-j\beta_{\mathrm{F}}^n(\omega)l} = g_n, \end{cases}$$

for each $n \in \mathbb{N}$.

Once the solution of the modal coefficients $\{a_{\mathrm{F}}^n(\omega), b_{\mathrm{F}}^n(\omega), a_{\mathrm{P}}^n(\omega), b_{\mathrm{P}}^n(\omega)\}_{n\in\mathbb{N}}$ have been computed, from (6)-(7), the surface impedance operator on boundary Γ_{I} can be defined as the trace of the pressure field associated to a prescribed normal velocity on Γ_{I}. This functional operator Z_{I} is completely described by

its action on the trace of each basis element φ_n as follows:

$$F = \sum_{n=0}^{\infty} f_n \varphi_n \mapsto Z_{\mathrm{I}} F = \sum_{n=0}^{\infty} Z_{\mathrm{I}}^n(\omega) f_n \varphi_n \quad \text{with} \quad Z_{\mathrm{I}}^n(\omega) = Z_{\mathrm{F}} \frac{a_{\mathrm{F}}^n(\omega) + b_{\mathrm{F}}^n(\omega)}{a_{\mathrm{F}}^n(\omega) - b_{\mathrm{F}}^n(\omega)}, \tag{8}$$

where Z_{F} is the characteristic impedance of the fluid medium. Analogously, the sound absorption coefficient of a porous layer can be computed as a scalar quantity associated to each transverse mode. So, for each mode $n \in \mathbb{N}$, the n-th modal sound absorption coefficient is given by

$$\alpha_n(\omega) = 1 - \left| \frac{Z_{\mathrm{I}}^n(\omega) - Z_{\mathrm{F}}}{Z_{\mathrm{I}}^n(\omega) + Z_{\mathrm{F}}} \right|^2 = 1 - \left| \frac{Y_{\mathrm{F}} - Y_{\mathrm{I}}^n(\omega)}{Y_{\mathrm{I}}^n(\omega) + Y_{\mathrm{F}}} \right|^2, \tag{9}$$

where the modal admittance values are given by $Y_{\mathrm{I}}^n(\omega) = 1/Z_{\mathrm{I}}^n(\omega)$ and the characteristic admittance by $Y_{\mathrm{F}} = 1/Z_{\mathrm{F}}$.

3. Acoustic characterization of a single porous layer using a fixed-frequency inverse problem

The main concern for practitioners consists in ensuring an adequate choice of the parametric porous model. The most accurate selection is not always possible to be known *a priori*, since it depends on the acoustic nature of the material samples. In fact, an inadequate model selection could ruins any parameter model fitting. As a partial remedy of these drawbacks, in the present work the proposed non-parametric methodology avoids the choice and the use of parametric models. In fact, it is not required to impose any functional dependency on the acoustic quantities used in (1)-(2) in terms of the frequency and it is only based on the experimental measurements. Throughout the following sections, four different strategies are described in detail, showing their drawbacks and the potential applicability for the characterization of the porous material properties.

3.1. Characterization with absorption datasets

In this first characterization strategy, for a fixed frequency value ω, it is assumed that the propagation problem (5) is solved with only a back admittance operator, whose coefficients $\{Y_{\mathrm{B}}^n(\omega)\}_{n\in\mathbb{N}}$ and the absorbing coefficients

$\{\alpha_n(\omega)\}_{n\in\mathbb{N}}$ are known. So, the characterization problem can be stated as follows.

Problem 3.1 (Inverse problem with a single absorption dataset)**.** *For a fixed frequency value ω and a fixed transverse mode n_0, find the complex-valued coefficients $k_{\mathrm{P}}(\omega)$ and $Z_{\mathrm{P}}(\omega)$ assuming only known the absorption value $\alpha_{n_0}(\omega)$ obtained by solving problem* (5) *with the back admittance value $Y_{\mathrm{B}}^{n_0}(\omega)$ on Γ_{B}.*

Lemma 3.2. *Problem 3.1 is ill-posed in the sense that there exists an innumerable number of solutions due to the lack of observation data.*

Proof. Firstly, despite $\alpha_{n_0}(\omega)$ only depends on the absolute value of a quotient of complex-valued expressions involving the surface admittance values, let us consider for simplicity the most favourable case where the surface admittance Y_{I} is also known in phase and modulus in addition to the absorption quantity. In this case, the pressure field Π_{P}, which is solution of the propagation problem (5), satisfies the boundary conditions

$$\frac{1}{j\omega\rho_{\mathrm{P}}(\omega)}\frac{\partial\Pi_{\mathrm{P}}}{\partial\boldsymbol{n}} = Y_{\mathrm{I}}\Pi_{\mathrm{P}} \quad \text{ on } \Gamma_{\mathrm{I}}, \qquad \frac{1}{j\omega\rho_{\mathrm{P}}(\omega)}\frac{\partial\Pi_{\mathrm{P}}}{\partial\boldsymbol{m}} = Y_{\mathrm{B}}\Pi_{\mathrm{P}} \quad \text{ on } \Gamma_{\mathrm{B}}.$$

Hence, the porous coefficients $a_{\mathrm{P}}^{n_0}$ and $b_{\mathrm{P}}^{n_0}$ hold

$$\begin{cases} -\dfrac{\beta_{\mathrm{P}}^{n_0}(\omega)}{\omega\rho_{\mathrm{P}}(\omega)}\left(-a_{\mathrm{P}}^{n_0}+b_{\mathrm{P}}^{n_0}\right) = Y_{\mathrm{I}}^{n_0}(\omega)\left(a_{\mathrm{P}}^{n_0}+b_{\mathrm{P}}^{n_0}\right), \\ \dfrac{\beta_{\mathrm{P}}^{n_0}(\omega)}{\omega\rho_{\mathrm{P}}(\omega)}\left(-a_{\mathrm{P}}^{n_0}e^{-j\beta_{\mathrm{P}}^{n_0}(\omega)d}+b_{\mathrm{P}}^{n_0}e^{j\beta_{\mathrm{P}}^{n}(\omega)d}\right) \\ \qquad = Y_{\mathrm{B}}^{n_0}(\omega)\left(a_{\mathrm{P}}^{n_0}e^{-j\beta_{\mathrm{P}}^{n_0}(\omega)d}+b_{\mathrm{P}}^{n_0}e^{j\beta_{\mathrm{P}}^{n_0}(\omega)d}\right), \end{cases}$$

where $Y_{\mathrm{I}}^{n_0}(\omega) = 1/Z_{\mathrm{I}}^{n_0}(\omega)$. From both equations, if the quotient $b_{\mathrm{P}}^{n_0}/a_{\mathrm{P}}^{n_0}$ is solved for both equations, it holds

$$\frac{Y_{\mathrm{B}}^{n_0}(\omega)+A(\omega)}{Y_{\mathrm{B}}^{n_0}(\omega)-A(\omega)B(\omega)} = \frac{A(\omega)+Y_{\mathrm{I}}^{n_0}(\omega)}{A(\omega)-Y_{\mathrm{I}}^{n_0}(\omega)}$$

with $A(\omega) = \beta_{\mathrm{P}}^{n_0}(\omega)/(\omega\rho_{\mathrm{P}}(\omega))$ and $B(\omega) = e^{2j\beta_{\mathrm{P}}^{n_0}(\omega)d}$. Obviously, the equation written above has uncountable solutions since, for each fixed arbitrary value of $B(\omega)$, there are different solution values for $A(\omega)$. The same conclusion is derived for the pair of coefficients $(\beta_{\mathrm{P}}^{n_0}(\omega), \rho_{\mathrm{P}}(\omega))$ and consequently also for

$(k_{\mathrm{P}}(\omega), Z_{\mathrm{P}}(\omega))$ taking into account the definition of wave number $\beta_{\mathrm{P}}^{n_0}$, this is, $k_{\mathrm{P}}(\omega) = \sqrt{(\beta_{\mathrm{P}}^{n_0}(\omega))^2 + \lambda_{n_0}^2}$ and $Z_{\mathrm{P}}(\omega) = \rho_{\mathrm{P}}(\omega) k_{\mathrm{P}}(\omega)/\omega$. □

The ill-posedness of the inverse problem stated above could be tentatively medicated adding new absorption observations with a second different back admittance leading to the following second strategy:

Problem 3.3 (Inverse problem with two absorption datasets)**.** *For a fixed frequency value ω and a fixed transverse mode n_0, find the complex-valued coefficients $k_{\mathrm{P}}(\omega)$ and $Z_{\mathrm{P}}(\omega)$ assuming known the absorption values $\alpha_{n_0}(\omega)$ and $\tilde{\alpha}_{n_0}(\omega)$ obtained respectively by solving problem* (5) *with two different back admittance values $Y_{\mathrm{B}}^{n_0}(\omega)$ and $\tilde{Y}_{\mathrm{B}}^{n_0}(\omega)$ on Γ_{B}.*

However, even with an additional absorption dataset, the inverse problem to be solved is still ill-posed.

Lemma 3.4. *Problem 3.3 is ill-posed in the sense that there exists an uncountable number of solutions due to the lack of phase information on the observation data.*

Proof. Firstly, let us consider for simplicity the most favourable case where the surface admittance Y_{I} and $\tilde{Y}_{\mathrm{I}}$ are known in phase and modulus in addition to the absorption quantities $\alpha_{n_0}(\omega)$ and $\tilde{\alpha}_{n_0}(\omega)$, respectively. In this case, the pressure fields Π_{P} and $\tilde{\Pi}_{\mathrm{P}}$, which are respectively solutions of propagation problem (5) with admittance operators Y_{B} and $\tilde{Y}_{\mathrm{B}}$, satisfy the boundary conditions

$$\frac{1}{j\omega\rho_{\mathrm{P}}(\omega)}\frac{\partial \Pi_{\mathrm{P}}}{\partial \boldsymbol{n}} = Y_{\mathrm{I}}\Pi_{\mathrm{P}} \quad \text{on } \Gamma_{\mathrm{I}}, \qquad \frac{1}{j\omega\rho_{\mathrm{P}}(\omega)}\frac{\partial \Pi_{\mathrm{P}}}{\partial \boldsymbol{m}} = Y_{\mathrm{B}}\Pi_{\mathrm{P}} \quad \text{on } \Gamma_{\mathrm{B}},$$
$$\frac{1}{j\omega\rho_{\mathrm{P}}(\omega)}\frac{\partial \tilde{\Pi}_{\mathrm{P}}}{\partial \boldsymbol{n}} = \tilde{Y}_{\mathrm{I}}\tilde{\Pi}_{\mathrm{P}} \quad \text{on } \Gamma_{\mathrm{I}}, \qquad \frac{1}{j\omega\rho_{\mathrm{P}}(\omega)}\frac{\partial \tilde{\Pi}_{\mathrm{P}}}{\partial \boldsymbol{m}} = \tilde{Y}_{\mathrm{B}}\tilde{\Pi}_{\mathrm{P}} \quad \text{on } \Gamma_{\mathrm{B}}.$$

Hence, the modal coefficients $a_{\mathrm{P}}^{n_0}$ and $b_{\mathrm{P}}^{n_0}$ associated to Π_{P} hold

$$\begin{cases} -\dfrac{\beta_{\mathrm{P}}^{n_0}(\omega)}{\omega\rho_{\mathrm{P}}(\omega)}\left(-a_{\mathrm{P}}^{n_0} + b_{\mathrm{P}}^{n_0}\right) = Y_{\mathrm{I}}^{n_0}(\omega)\left(a_{\mathrm{P}}^{n_0} + b_{\mathrm{P}}^{n_0}\right), \\ \dfrac{\beta_{\mathrm{P}}^{n_0}(\omega)}{\omega\rho_{\mathrm{P}}(\omega)}\left(-a_{\mathrm{P}}^{n_0} e^{-j\beta_{\mathrm{P}}^{n_0}(\omega)d} + b_{\mathrm{P}}^{n_0} e^{j\beta_{\mathrm{P}}^{n_0}(\omega)d}\right) \\ \qquad = Y_{\mathrm{B}}^{n_0}(\omega)\left(a_{\mathrm{P}}^{n_0} e^{-j\beta_{\mathrm{P}}^{n_0}(\omega)d} + b_{\mathrm{P}}^{n_0} e^{j\beta_{\mathrm{P}}^{n_0}(\omega)d}\right), \end{cases}$$

and analogously those modal coefficients $\tilde{a}_{\mathrm{P}}^{n_0}$ and $\tilde{b}_{\mathrm{P}}^{n_0}$ associated to $\tilde{\Pi}_{\mathrm{P}}$ hold

$$\begin{cases} -\dfrac{\beta_{\mathrm{P}}^{n_0}(\omega)}{\omega\rho_{\mathrm{P}}(\omega)}\left(-\tilde{a}_{\mathrm{P}}^{n_0}+\tilde{b}_{\mathrm{P}}^{n_0}\right)=\tilde{Y}_{\mathrm{I}}^{n_0}(\omega)\left(\tilde{a}_{\mathrm{P}}^{n_0}+\tilde{b}_{\mathrm{P}}^{n_0}\right), \\ \dfrac{\beta_{\mathrm{P}}^{n_0}(\omega)}{\omega\rho_{\mathrm{P}}(\omega)}\left(-\tilde{a}_{\mathrm{P}}^{n_0}e^{-j\beta_{\mathrm{P}}^{n_0}(\omega)d}+\tilde{b}_{\mathrm{P}}^{n_0}e^{j\beta_{\mathrm{P}}^{n_0}(\omega)d}\right) \\ \qquad =\tilde{Y}_{\mathrm{B}}^{n_0}(\omega)\left(\tilde{a}_{\mathrm{P}}^{n_0}e^{-j\beta_{\mathrm{P}}^{n_0}(\omega)d}+\tilde{b}_{\mathrm{P}}^{n_0}e^{j\beta_{\mathrm{P}}^{n_0}(\omega)d}\right), \end{cases}$$

where $Y_{\mathrm{I}}^{n_0}(\omega)=1/Z_{\mathrm{I}}^{n_0}(\omega)$ and $\tilde{Y}_{\mathrm{I}}^{n_0}(\omega)=1/\tilde{Z}_{\mathrm{I}}^{n_0}(\omega)$. Following straightforward computations (analogous to those ones described, for instance, in [14] where impedance-dependent expressions are used instead), it leads to

$$A(\omega)=\sqrt{\frac{Y_{\mathrm{I}}^{n_0}(\omega)\tilde{Y}_{\mathrm{I}}^{n_0}(\omega)\left(\tilde{Y}_{\mathrm{B}}^{n_0}(\omega)-Y_{\mathrm{B}}^{n_0}(\omega)\right)+Y_{\mathrm{B}}^{n_0}(\omega)\tilde{Y}_{\mathrm{B}}^{n_0}(\omega)\left(\tilde{Y}_{\mathrm{I}}^{n_0}(\omega)-Y_{\mathrm{I}}^{n_0}(\omega)\right)}{\left(\tilde{Y}_{\mathrm{B}}^{n_0}(\omega)-Y_{\mathrm{B}}^{n_0}(\omega)\right)+\left(\tilde{Y}_{\mathrm{I}}^{n_0}(\omega)-Y_{\mathrm{I}}^{n_0}(\omega)\right)}}, \tag{10}$$

$$\beta_{\mathrm{P}}^{n_0}(\omega)=\frac{1}{2jd}\ln\left(\frac{Y_{\mathrm{I}}^{n_0}(\omega)-A(\omega)}{Y_{\mathrm{I}}^{n_0}(\omega)+A(\omega)}\frac{Y_{\mathrm{B}}^{n_0}(\omega)-A(\omega)}{Y_{\mathrm{B}}^{n_0}(\omega)+A(\omega)}\right), \qquad \rho_{\mathrm{P}}(\omega)=\frac{\beta_{\mathrm{P}}^{n_0}(\omega)}{\omega A(\omega)}, \tag{11}$$

and consequently there exists a solution for $k_{\mathrm{P}}(\omega)$ and $Z_{\mathrm{P}}(\omega)$ (given by $k_{\mathrm{P}}(\omega)=\sqrt{(\beta_{\mathrm{P}}^{n_0}(\omega))^2+\lambda_{n_0}^2}$ and $Z_{\mathrm{P}}(\omega)=\rho_{\mathrm{P}}(\omega)k_{\mathrm{P}}(\omega)/\omega$).

Now, coming back to the original absorption datasets of Problem 3.3, it is easy to show that the inverse problem is ill-posed using the solution described above: since $\alpha_{n_0}(\omega)$ (9) only depends on the absolute value of a complex-valued expressions, if the value of $Y_{\mathrm{I}}^{n_0}(\omega)$ in (9) is replaced by

$$Y_{\mathrm{F}}\frac{Y_{\mathrm{F}}(e^{i\gamma}-1)-Y_{\mathrm{I}}^{n_0}(\omega)(e^{i\gamma}+1)}{Y_{\mathrm{I}}^{n_0}(\omega)(e^{i\gamma}-1)-Y_{\mathrm{F}}(e^{i\gamma}+1)},$$

for any arbitrary value $\gamma\in(-\pi,\pi]$, then the absorption values will be identical for any arbitrary value of γ. The same argument can be applied to the absorption coefficient $\tilde{\alpha}_{n_0}(\omega)$ replacing the values of $\tilde{Y}_{\mathrm{I}}^{n_0}(\omega)$ in (9). In conclusion, the inverse problem based on absorption datasets have an infinity uncountable number of solutions varying simply γ. □

3.2. Characterization with surface impedance datasets

In this third characterization strategy, for a fixed frequency value ω, it is assumed that only a propagation problem (5) is solved with only a back admit-

tance operator, whose coefficients are $\{Y_{\mathrm{B}}^n(\omega)\}_{n\in\mathbb{N}}$ and the surface admittance values $\{Y_{\mathrm{I}}^n(\omega)\}_{n\in\mathbb{N}}$ are known. So, the characterization problem can be stated as follows.

Problem 3.5 (Inverse problem with a single surface admittance dataset)**.** *For a fixed frequency value ω and a fixed transverse mode n_0, find the complex-valued coefficients $k_{\mathrm{P}}(\omega)$ and $Z_{\mathrm{P}}(\omega)$ assuming only known the surface admittance value $Y_{\mathrm{I}}^{n_0}(\omega)$ on Γ_{I} obtained by solving problem* (5) *with the back admittance value $Y_{\mathrm{B}}^{n_0}(\omega)$ on Γ_{B}.*

Lemma 3.6. *Problem 3.5 is ill-posed in the sense that there exist innumerable solutions due to the lack of observation data.*

Proof. The same arguments described in the proof of Lemma 3.2 lead to the conclusion that there exists an uncountable number of solutions. □

The ill-posedness of the inverse problem stated above can be overcome adding an additional surface admittance observation with a second different back admittance leading to the fourth characterization approach:

Problem 3.7 (Inverse problem with two surface impedance datasets)**.** *For a fixed frequency value ω and a fixed transverse mode n_0, find the complex-valued coefficients $k_{\mathrm{P}}(\omega)$ and $Z_{\mathrm{P}}(\omega)$ assuming known the surface admittance values $Y_{\mathrm{I}}^{n_0}(\omega)$ and $\tilde{Y}_{\mathrm{I}}^{n_0}(\omega)$ on Γ_{I} obtained respectively by solving problem* (5) *with two different back admittance values $Y_{\mathrm{B}}^{n_0}(\omega)$ and $\tilde{Y}_{\mathrm{B}}^{n_0}(\omega)$ on Γ_{B}.*

However, even with an additional surface impedance dataset, the inverse problem to be solved will have an infinity (but countable) number of solutions.

Lemma 3.8. *Problem 3.7 is well-posed in the sense that there exists an infinite (but countable) number of solutions due to the periodicity of the wave number values.*

Proof. Following identical arguments to those ones used in the proof of Lemma 3.4, the existence of solution of the inverse problem is ensured from the expressions

of $A(\omega)$, $\beta_{\mathrm{P}}^{n_0}(\omega)$ and $\rho_{\mathrm{P}}(\omega)$ in (10)-(11). Uniqueness of solution for the expression $A(\omega)$ is straightforward taking into account that it is the root of a quadratic polynomial, where only the solution with positive real part is considered. However, from (11), it is clear that due to the periodicity (with respect to the imaginary axis) of the complex-valued exponential function, the wave number admits the solutions

$$\beta_{\mathrm{P}}^{n_0}(\omega) = \frac{1}{2jd} \ln \left(\frac{Y_{\mathrm{I}}^{n_0}(\omega) - A(\omega)}{Y_{\mathrm{I}}^{n_0}(\omega) + A(\omega)} \frac{Y_{\mathrm{B}}^{n_0}(\omega) - A(\omega)}{Y_{\mathrm{B}}^{n_0}(\omega) + A(\omega)} \right) + \frac{\pi \ell}{d} \qquad \text{for } \ell \in \mathbb{Z}, \quad (12)$$

which leads to an infinity (but countable) number of solutions for $\beta_{\mathrm{P}}^{n_0}(\omega)$. The same conclusions hold for $\rho_{\mathrm{P}}(\omega)$ and $Z_{\mathrm{P}}(\omega)$. □

Remark 3.9. *To overcome the lack of uniqueness in the previous inverse problem, the value of the integer parameter ℓ should be fixed. In that case, the inverse Problem 3.7 would be well-posed and it would have a unique solution. For this purpose, two assumptions are considered: (i) the frequency response function associated to $\beta_{\mathrm{P}}^{n_0}(\omega)$ is continuous (so, no jumps are allowed in its frequency response) and (ii) the value of parameter ℓ is assumed known at a given frequency value.*

Taking into account the strategy devised in Remark 3.9, to overcome the lack of uniqueness of solution in (11), it is enough to know the low frequency limit of the dynamic mass density, i.e., $\lim_{\omega \to 0} \rho_{\mathrm{P}}(\omega) = \rho_{\mathrm{P}0}$ (see for instance, the relevance of this low-frequency limits for rigid and limp frame porous materials in [23, 24]).

4. Acoustic characterization of a double porous layer using a fixed-frequency inverse problem

In most of the acoustic engineering applications, absorbing materials are stratified and hence they are composed by a number of different porous layers. The characterization strategy described in the previous section can be adapted to deal with this multilayer configuration. For the sake of conciseness, a double multilayer configuration composed with two different porous materials is

presented in this section. However, analogous arguments could be applied to stratified porous media with a higher number of layers.

4.1. Statement of the direct propagation problem

The mathematical model of the time-harmonic wave propagation problem is analogous to (5) described in Section 2.3 for a single layer case. More precisely, for a double layer configuration, let Ω_{F} be three-dimensional domain occupied by the fluid and Ω_{P} and Ω_{Q} be respectively the three-dimensional domains occupied by two porous layers (see Figure 3 for a better understanding of the notation). The coupling boundary between both porous layers is denoted by Γ_{P}, located on the plane $x_1 = h$. Notation on the rest of exterior and coupling boundaries and also on the unit normal vectors is identical to that one used in Section 3.

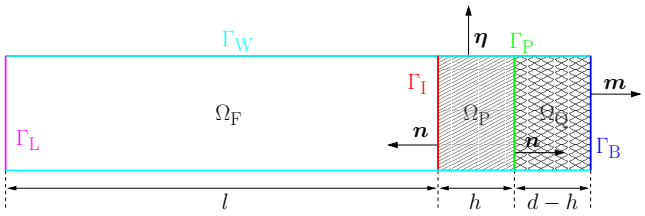

Figure 3: Schematic two-dimensional cut of the impedance tube where the fluid and the two porous subdomains, Ω_{F}, Ω_{P}, and Ω_{Q}, are marked with different patterns. The boundaries are highlighted also with different colours: Γ_{I} in red, Γ_{W} in cyan, Γ_{L} in magenta, Γ_{P} in green, and Γ_{B} in blue.

Hence, the strong differential formulation of the coupled problem with a double porous layer is given by the following problem: for a fixed angular frequency $\omega > 0$, a prescribed back surface admittance operator Y_{B}, and an acoustic loudspeaker source G, find the fluid pressure field Π_{F} and the porous pressure fields

Π_{P} and Π_{Q} such that

$$\begin{cases} -k_{\mathrm{F}}^2(\omega)\Pi_{\mathrm{F}} - \Delta\Pi_{\mathrm{F}} = 0 & \text{in } \Omega_{\mathrm{F}}, \\ -k_{\mathrm{P}}^2(\omega)\Pi_{\mathrm{P}} - \Delta\Pi_{\mathrm{P}} = 0 & \text{in } \Omega_{\mathrm{P}}, \\ -k_{\mathrm{Q}}^2(\omega)\Pi_{\mathrm{Q}} - \Delta\Pi_{\mathrm{Q}} = 0 & \text{in } \Omega_{\mathrm{Q}}, \\ \dfrac{1}{\rho_{\mathrm{F}}}\dfrac{\partial\Pi_{\mathrm{F}}}{\partial\boldsymbol{n}} = \dfrac{1}{\rho_{\mathrm{P}}(\omega)}\dfrac{\partial\Pi_{\mathrm{P}}}{\partial\boldsymbol{n}} & \text{on } \Gamma_{\mathrm{I}}, \\ \Pi_{\mathrm{F}} = \Pi_{\mathrm{P}} & \text{on } \Gamma_{\mathrm{I}}, \\ \dfrac{1}{\rho_{\mathrm{P}}(\omega)}\dfrac{\partial\Pi_{\mathrm{P}}}{\partial\boldsymbol{n}} = \dfrac{1}{\rho_{\mathrm{Q}}(\omega)}\dfrac{\partial\Pi_{\mathrm{Q}}}{\partial\boldsymbol{n}} & \text{on } \Gamma_{\mathrm{P}}, \\ \Pi_{\mathrm{P}} = \Pi_{\mathrm{Q}} & \text{on } \Gamma_{\mathrm{P}}, \\ \dfrac{1}{j\omega\rho_{\mathrm{Q}}(\omega)}\dfrac{\partial\Pi_{\mathrm{Q}}}{\partial\boldsymbol{m}} = Y_{\mathrm{B}}\Pi_{\mathrm{Q}} & \text{on } \Gamma_{\mathrm{B}}, \\ \dfrac{\partial\Pi_{\mathrm{F}}}{\partial\boldsymbol{\eta}} = 0 & \text{on } \Gamma_{\mathrm{W}} \cap \partial\Omega_{\mathrm{F}}, \\ \dfrac{\partial\Pi_{\mathrm{P}}}{\partial\boldsymbol{\eta}} = 0 & \text{on } \Gamma_{\mathrm{W}} \cap \partial\Omega_{\mathrm{P}}, \\ \dfrac{\partial\Pi_{\mathrm{Q}}}{\partial\boldsymbol{\eta}} = 0 & \text{on } \Gamma_{\mathrm{W}} \cap \partial\Omega_{\mathrm{Q}}, \\ \Pi_{\mathrm{F}} = G & \text{on } \Gamma_{\mathrm{L}}, \end{cases} \tag{13}$$

where $k_{\mathrm{F}}(\omega) = \omega/c_{\mathrm{F}}$ being ρ_{F} and c_{F} the mass density and the sound velocity in the fluid, $\rho_{\mathrm{P}}(\omega)$, $\rho_{\mathrm{Q}}(\omega)$ and $k_{\mathrm{P}}(\omega)$, $k_{\mathrm{Q}}(\omega)$ are the frequency-dependent equivalent dynamic mass density and the frequency-dependent wave number of the porous materials located respectively in the layers Ω_{P} and Ω_{Q}. Vectors $\boldsymbol{n}$, $\boldsymbol{m}$, and $\boldsymbol{\eta}$ are respectively the unitary and normal on boundaries $\Gamma_{\mathrm{I}} \cup \Gamma_{\mathrm{P}}$, Γ_{B}, and Γ_{W}, and outward to the porous layer Ω_{P} (on the boundaries where it is applicable).

The direct propagation problem (13) can be decoupled in terms of the transverse modes (as it has been described in detail for a single layer in Section 3). Consequently, the modal coefficients $\{a_{\mathrm{F}}^n, b_{\mathrm{F}}^n, a_{\mathrm{P}}^n, b_{\mathrm{P}}^n, a_{\mathrm{Q}}^n, b_{\mathrm{Q}}^n\}_{n\in\mathbb{N}}$ associated respectively to the pressure fields Π_{F}, Π_{P}, and Π_{Q} are solution of the following

sequence of linear algebraic system of equations: for each $n \in \mathbb{N}$, it holds

$$\begin{cases} \rho_{\mathrm{P}}(\omega)\beta_{\mathrm{F}}^n(\omega)(-a_{\mathrm{F}}^n + b_{\mathrm{F}}^n) = \rho_{\mathrm{F}}\beta_{\mathrm{P}}^n(\omega)(-a_{\mathrm{P}}^n + b_{\mathrm{P}}^n), \\ a_{\mathrm{F}}^n + b_{\mathrm{F}}^n = a_{\mathrm{P}}^n + b_{\mathrm{P}}^n, \\ \rho_{\mathrm{Q}}(\omega)\beta_{\mathrm{P}}^n(\omega)(-a_{\mathrm{P}}^n e^{-j\beta_{\mathrm{P}}^n(\omega)h} + b_{\mathrm{P}}^n e^{j\beta_{\mathrm{P}}^n(\omega)h}) \\ \qquad\qquad = \rho_{\mathrm{P}}(\omega)\beta_{\mathrm{Q}}^n(\omega)(-a_{\mathrm{Q}}^n e^{-j\beta_{\mathrm{Q}}^n(\omega)h} + b_{\mathrm{Q}}^n e^{j\beta_{\mathrm{Q}}^n(\omega)h}), \\ a_{\mathrm{P}}^n e^{-j\beta_{\mathrm{P}}^n(\omega)h} + b_{\mathrm{P}}^n e^{j\beta_{\mathrm{P}}^n(\omega)h} = a_{\mathrm{Q}}^n e^{-j\beta_{\mathrm{Q}}^n(\omega)h} + b_{\mathrm{Q}}^n e^{j\beta_{\mathrm{Q}}^n(\omega)h}, \\ \dfrac{\beta_{\mathrm{Q}}^n(\omega)}{\omega\rho_{\mathrm{Q}}(\omega)}\left(-a_{\mathrm{Q}}^n e^{-j\beta_{\mathrm{Q}}^n(\omega)d} + b_{\mathrm{Q}}^n e^{j\beta_{\mathrm{Q}}^n(\omega)d}\right) = Y_{\mathrm{B}}^n(\omega)\left(a_{\mathrm{Q}}^n e^{-j\beta_{\mathrm{Q}}^n(\omega)d} + b_{\mathrm{Q}}^n e^{j\beta_{\mathrm{Q}}^n(\omega)d}\right), \\ a_{\mathrm{F}}^n e^{j\beta_{\mathrm{F}}^n(\omega)l} + b_{\mathrm{F}}^n e^{-j\beta_{\mathrm{F}}^n(\omega)l} = g_n, \end{cases} \tag{14}$$

where the notation is analogous to that one used in problem (6)-(7), and $\beta_{\mathrm{Q}}^n(\omega) = \sqrt{k_{\mathrm{Q}}^2(\omega) - \lambda_n^2}$ for $n \in \mathbb{N}$. Once these modal coefficients are computed solving the above linear system for a fixed $n \in \mathbb{N}$, the contribution of the n-th mode to the surface impedance (8) on Γ_{I} or the absorption coefficient (9) of the double porous layer configuration can be computed straightforwardly.

4.2. Characterization with four surface admittance datasets

In the sections presented above, Problems 3.1, 3.3, 3.5, and 3.7 deal with the characterization of a single porous layer. However, the numerical methodology proposed in this work can be applied to frameworks much more complex where two porous materials can be characterized simultaneously. Obviously, the datasets to be used in the inverse problem should be also doubled. Notice also that the present strategy combined with a Transfer Matrix Method (TMM) [3, Chapter 11] applied to each modal contribution could be used in a general multilayer configuration but at the expense of increasing the number of datasets used in the inverse characterization problem.

Consequently, for a multilayer formed by two layers of different porous materials with characteristic impedance and wave number pairs $(Z_{\mathrm{P}}(\omega), k_{\mathrm{P}}(\omega))$ and $(Z_{\mathrm{Q}}(\omega), k_{\mathrm{Q}}(\omega))$, respectively, the characterization problem can be stated as follows.

Problem 4.1 (Inverse problem with four surface impedance datasets)**.** *For a fixed frequency value ω and a fixed transverse mode n_0, find the complex-valued coefficients of the characteristic impedance and the wave number $(Z_{\mathrm{P}}(\omega), k_{\mathrm{P}}(\omega))$ and $(Z_{\mathrm{Q}}(\omega), k_{\mathrm{Q}}(\omega))$, associated to the two porous layers assuming known:*

(i) The surface admittance values $Y_{\mathrm{I}}^{n_0}(\omega)$ on Γ_{I}, obtained respectively by solving a single layer configuration problem (5) *with the porous material $(Z_{\mathrm{P}}(\omega), k_{\mathrm{P}}(\omega))$ and the back admittance values $Y_{\mathrm{B}}^{n_0}(\omega)$ on Γ_{B}.*

(ii) The surface admittance values $\tilde{Y}_{\mathrm{I}}^{n_0}(\omega)$ on Γ_{I}, obtained respectively by solving a single layer configuration problem (5) *with the porous material $(Z_{\mathrm{Q}}(\omega), k_{\mathrm{Q}}(\omega))$ and the back admittance values $\tilde{Y}_{\mathrm{B}}^{n_0}(\omega)$ on Γ_{B}.*

(iii) The surface admittance values $\hat{Y}_{\mathrm{I}}^{n_0}(\omega)$ on Γ_{I}, obtained respectively by solving a double layer configuration problem (13)*, being $(Z_{\mathrm{P}}(\omega), k_{\mathrm{P}}(\omega))$ the coefficients of the first porous layer, the second one corresponding to $(Z_{\mathrm{Q}}(\omega), k_{\mathrm{Q}}(\omega))$, and the back admittance value $\hat{Y}_{\mathrm{B}}^{n_0}(\omega)$ on Γ_{B}.*

(iv) The surface admittance values $\breve{Y}_{\mathrm{I}}^{n_0}(\omega)$ on Γ_{I}, obtained respectively by solving a double layer configuration problem (13) *with the double layer configuration of dataset (iii) inverted, being $(Z_{\mathrm{Q}}(\omega), k_{\mathrm{Q}}(\omega))$ now the coefficients of the first porous layer, the second one corresponding thus to $(Z_{\mathrm{P}}(\omega), k_{\mathrm{P}}(\omega))$, and the back admittance value $\breve{Y}_{\mathrm{B}}^{n_0}(\omega)$ on Γ_{B}.*

Remark 4.2. *Other choices of surface admittance datasets could be considered in definition of Problem 4.1 (for instance, datasets involving only double layer configurations and two different back admittance conditions). In fact, since single and double layer configurations are used in Problem 4.1, the same back admittance operator could be considered in all the datasets i)-iv).*

As it is expected from the results shown related to Problem 3.7, even with the use of four surface impedance datasets, the inverse problem characterizing the double layer configuration has an infinity (but countable) number of solutions.

Lemma 4.3. *Problem 4.1 is well-posed in the sense that there exists an infinite (but countable) number of solutions due to the periodicity of the wave number values.*

Proof. Firstly, consider the datasets i) and iii) and assume that the complex-valued properties $(Z_{\rm Q}(\omega), k_{\rm Q}(\omega))$ are known. For instance, from dataset iii) can be understood as the surface admittance data coming from a single layer configuration where the back admittance data can be computed as the input admittance of the porous layer $(Z_{\rm P}(\omega), k_{\rm P}(\omega))$ backed with the admittance $\tilde{Y}_{\rm B}^{n_0}(\omega)$. More precisely, the back surface admittance on $\Gamma_{\rm P}$ associated to the front boundary of a layer of porous material $(Z_{\rm Q}(\omega), k_{\rm Q}(\omega))$ of thickness $d-h$ and supported on its back-end boundary with admittance $\tilde{Y}_{\rm B}^{n_0}(\omega)$ is given by

$$\tilde{\tilde{Y}}_{\rm B}^{n_0}(\omega) = \frac{1}{Y_{\rm Q}(\omega)} \frac{Y_{\rm Q}(\omega) + \tilde{Y}_{\rm B}^{n_0}(\omega)\tanh(\beta_{\rm Q}^{n_0}(\omega)(d-h))}{\tilde{Y}_{\rm B}^{n_0}(\omega) + Y_{\rm Q}(\omega)\tanh(\beta_{\rm Q}^{n_0}(\omega)(d-h)}, \tag{15}$$

where $Y_{\rm Q}(\omega) = 1/Z_{\rm Q}(\omega)$. Hence, applying the arguments of the proof in Lemma 3.8, the values $(Z_{\rm P}(\omega), k_{\rm P}(\omega)))$ are uniquely determined except for the phase changes in the wave number coefficient (see (12)). Analogous arguments are also applicable to dataset i).

Once the phase of the wave number is fixed using a given criterion (see Remark 3.9), the existence and uniqueness of solution of single layer Problem 3.7 with datasets i) and iii) ensures that the mapping $\mathcal{X} : (Z_{\rm Q}, k_{\rm Q}) \mapsto (Z_{\rm P}, k_{\rm P})$ is well-defined and injective. In addition, since expressions involved in (10)-(11) and (15) are continuous, this mapping is also continuous in $\mathbb{C}^2$. Analogous arguments can be used to conclude that if $(Z_{\rm P}, k_{\rm P})$ are assumed known then the complex-valued coefficients $(Z_{\rm Q}, k_{\rm Q})$ can be uniquely determined from datasets ii) and iv) (except for the phase changes in the wave number coefficient). Hence, the mapping $\mathcal{Y} : (Z_{\rm P}, k_{\rm P}) \mapsto (Z_{\rm Q}, k_{\rm Q})$ is well-defined, injective and continuous. In addition, since the single layer problems which are involved in mappings $\mathcal{X}$ and $\mathcal{Y}$ involves datasets iii) and iv) respectively, for an arbitrary complex disc $D \subset \mathbb{C}^2$, it holds $\mathcal{X}(\mathcal{Y}(D)) = D$ (otherwise, it would imply that one of the datasets is not compatible with the rest of them).

Consequently, the inverse Problem 4.1 can be formulated as a fixed point problem: find $(Z_{\mathrm{P}}(\omega), k_{\mathrm{P}}(\omega))$ such that $(Z_{\mathrm{P}}(\omega), k_{\mathrm{P}}(\omega)) = (\mathcal{X} \circ \mathcal{Y})(Z_{\mathrm{P}}(\omega), k_{\mathrm{P}}(\omega))$. Hence, the existence of solution is guaranteed from the classical Brouwer fixed-point theorem [25] applied on a disc of sufficient large radius D in $\mathbb{C}^2$. Uniqueness of this fixed point is clear from the injective character of $\mathcal{X}$ and $\mathcal{Y}$. Once $(Z_{\mathrm{P}}(\omega), k_{\mathrm{P}}(\omega))$ is determined, the values of $(Z_{\mathrm{Q}}(\omega), k_{\mathrm{Q}}(\omega))$ are computed straightforwardly by means of $(Z_{\mathrm{Q}}(\omega), k_{\mathrm{Q}}(\omega) = \mathcal{Y}(Z_{\mathrm{P}}(\omega), k_{\mathrm{P}}(\omega))$. In conclusion, except for a phase change in the wave numbers (which leads to a countable infinite number of solutions on $k_{\mathrm{P}}(\omega)$ and $k_{\mathrm{Q}}(\omega)$), the inverse Problem 4.1 is well-posed. □

Despite the proof of uniqueness and existence of Problem 4.1 relies on the use of a fixed-point theorem, the numerical resolution of both inverse Problems 3.7 and 4.1, (with single and double layer configurations) involves the same numerical method whose main characteristics are: the rewritten of the modal linear system in terms of robust primal unknowns and the use of a TMM method combined with a derivative-free optimization method to find the solution of each inverse problem. This numerical procedure is described in detail in the following section.

5. Numerical procedure to solve the inverse problems

The proposed approach for determining the characteristic impedance and the wave number associated to a fluid-equivalent rigid porous model uses intensively the numerical solution of sequence of inverse problems, which fits a discrete set of frequency-dependent experimental measurements of the surface admittance of a single or double layer configuration. With this aim, for a fixed frequency value and a given modal contribution, the inverse problem is rewritten as a minimization problem where the cost function is the relative error between the experimental measurements and the surface admittance computed with the direct propagation problem.

Since the fluid-equivalent equations can be written in terms of any pair of the dynamic coefficients introduced in Section 2.3, there exists a variety of

model coefficients which could be used as primal unknowns in the cost function used in the minimization problem to be solved numerically. For instance, the surface admittance could be computed naively in terms of the real and the imaginary part of the mass density $\rho_{\mathrm{P}}(\omega)$ and the bulk modulus $K_{\mathrm{P}}(\omega)$ as primal unknowns. In this case, despite the fitting relative error is almost negligible, spurious oscillations distort the parameter frequency-response due to the exponential dependency of the TMM matrix coefficients with respect to these acoustic quantities (see [26] for details).

In order to mitigate this situation, instead of using the dynamic mass density and the dynamic bulk modulus as primal unknowns, the minimization problem has been rewritten replacing the real and imaginary part of the bulk modulus by a novel pair of primal unknowns: $\delta_{\mathrm{P}}(\omega) = \mathrm{Re}(\beta_{\mathrm{P}}^{n_0}(\omega))d$ and $M_{\mathrm{P}}(\omega) = e^{\mathrm{Im}(\beta_{\mathrm{P}}^{n_0}(\omega))d}$, which involves the wave number $\beta_{\mathrm{P}}^{n_0}(\omega)$ of the porous material associated to the n_0-th transverse mode and the thickness of the porous layer d. Hence, since the acoustic quantity measurements chosen for fitting is the surface admittance in Problem 3.7, the values of $M_{\mathrm{P}}(\omega)$, $\delta_{\mathrm{P}}(\omega)$, $\mathrm{Re}(\rho_{\mathrm{P}}(\omega))$, and $\mathrm{Im}(\rho_{\mathrm{P}}(\omega))$ are computed as the solution of the minimization problem

$$
\begin{aligned}
&(M_{\mathrm{P}}(\omega), \delta_{\mathrm{P}}(\omega), \mathrm{Re}(\rho_{\mathrm{P}}(\omega)), \mathrm{Im}(\rho_{\mathrm{P}}(\omega))) \\
&\quad = \underset{\substack{M_{\mathrm{P}},\delta_{\mathrm{P}}>0 \\ \mathrm{Re}(\rho_{\mathrm{P}})>0 \\ \mathrm{Im}(\rho_{\mathrm{P}})<0}}{\arg\min} \left(\frac{|Y_{\mathrm{I}}(\omega) - Y_{\mathrm{I}}^{\mathrm{TMM}}(\omega, n_0, Y_{\mathrm{B}}^{n_0}(\omega), M_{\mathrm{P}}, \delta_{\mathrm{P}}, \mathrm{Re}(\rho_{\mathrm{P}}), \mathrm{Im}(\rho_{\mathrm{P}}))|^2}{|Y_{\mathrm{I}}(\omega)|^2} \right. \\
&\qquad\qquad \left. + \frac{|\tilde{Y}_{\mathrm{I}}(\omega) - Y_{\mathrm{I}}^{\mathrm{TMM}}(\omega, n_0, \tilde{Y}_{\mathrm{B}}^{n_0}(\omega), M_{\mathrm{P}}, \delta_{\mathrm{P}}, \mathrm{Re}(\rho_{\mathrm{P}}), \mathrm{Im}(\rho_{\mathrm{P}}))|^2}{|\tilde{Y}_{\mathrm{I}}(\omega)|^2} \right),
\end{aligned}
\tag{16}
$$

where $Y_{\mathrm{I}}^{\mathrm{TMM}}(\omega, n_0, Y_{\mathrm{B}}^{n_0}, M_{\mathrm{P}}, \delta_{\mathrm{P}}, \mathrm{Re}(\rho_{\mathrm{P}}), \mathrm{Im}(\rho_{\mathrm{P}}))$ is the surface admittance computed by solving the linear problem (5) (single layer configuration) with back admittance $Y_{\mathrm{B}}^{n_0}$ using the TMM method for the n_0-th modal contribution. Similarly, the minimization problem with a double multilayer configuration can be

written as follows:

$$
\begin{aligned}
&(M_{\mathrm{P}}(\omega), M_{\mathrm{Q}}(\omega), \delta_{\mathrm{P}}(\omega), \delta_{\mathrm{Q}}(\omega), \mathrm{Re}(\rho_{\mathrm{P}}(\omega)), \mathrm{Re}(\rho_{\mathrm{Q}}(\omega)), \mathrm{Im}(\rho_{\mathrm{P}}(\omega)), \mathrm{Im}(\rho_{\mathrm{Q}}(\omega))) \\
&= \underset{\substack{M_{\mathrm{P}}, M_{\mathrm{Q}}, \delta_{\mathrm{P}}, \delta_{\mathrm{Q}} > 0 \\ \mathrm{Re}(\rho_{\mathrm{P}}), \mathrm{Re}(\rho_{\mathrm{Q}}) > 0 \\ \mathrm{Im}(\rho_{\mathrm{P}}), \mathrm{Im}(\rho_{\mathrm{Q}}) < 0}}{\arg\min} \Bigg(\frac{|Y_{\mathrm{I}}(\omega) - Y_{\mathrm{I}}^{\mathrm{TMM}}(\omega, n_0, Y_{\mathrm{B}}^{n_0}(\omega), M_{\mathrm{P}}, \delta_{\mathrm{P}}, \mathrm{Re}(\rho_{\mathrm{P}}), \mathrm{Im}(\rho_{\mathrm{P}}))|^2}{|Y_{\mathrm{I}}(\omega)|^2} \\
&\quad + \frac{|\tilde{Y}_{\mathrm{I}}(\omega) - Y_{\mathrm{I}}^{\mathrm{TMM}}(\omega, n_0, \tilde{Y}_{\mathrm{B}}^{n_0}(\omega), M_{\mathrm{Q}}, \delta_{\mathrm{Q}}, \mathrm{Re}(\rho_{\mathrm{Q}}), \mathrm{Im}(\rho_{\mathrm{Q}}))|^2}{|\tilde{Y}_{\mathrm{I}}(\omega)|^2} \\
&\quad + \frac{|\hat{Y}_{\mathrm{I}}(\omega) - Y_{\mathrm{I}}^{\mathrm{TMM}}(\omega, n_0, \hat{Y}_{\mathrm{B}}^{n_0}(\omega), M_{\mathrm{P}}, M_{\mathrm{Q}}, \delta_{\mathrm{P}}, \delta_{\mathrm{Q}}, \mathrm{Re}(\rho_{\mathrm{P}}), \mathrm{Re}(\rho_{\mathrm{Q}}), \mathrm{Im}(\rho_{\mathrm{P}}), \mathrm{Im}(\rho_{\mathrm{Q}}))|^2}{|\hat{Y}_{\mathrm{I}}(\omega)|^2} \\
&\quad + \frac{|\breve{Y}_{\mathrm{I}}(\omega) - Y_{\mathrm{I}}^{\mathrm{TMM}}(\omega, n_0, \breve{Y}_{\mathrm{B}}^{n_0}(\omega), M_{\mathrm{P}}, M_{\mathrm{Q}}, \delta_{\mathrm{P}}, \delta_{\mathrm{Q}}, \mathrm{Re}(\rho_{\mathrm{P}}), \mathrm{Re}(\rho_{\mathrm{Q}}), \mathrm{Im}(\rho_{\mathrm{P}}), \mathrm{Im}(\rho_{\mathrm{Q}}))|^2}{|\breve{Y}_{\mathrm{I}}(\omega)|^2} \Bigg),
\end{aligned}
\tag{17}
$$

where $\delta_{\mathrm{Q}}(\omega) = \mathrm{Re}(\beta_{\mathrm{Q}}^{n_0}(\omega))(d-h)$ and $M_{\mathrm{Q}}(\omega) = e^{\mathrm{Im}(\beta_{\mathrm{Q}}^{n_0}(\omega))(d-h)}$ are the pair of primal unknowns related to the second porous layer involving its wave number $\beta_{\mathrm{Q}}^{n_0}$ and its thickness $d-h$ and $Y_{\mathrm{I}}^{\mathrm{TMM}}$ denotes the surface admittance computed by solving the linear problem (13) (double multilayer configuration) with back admittance $\tilde{Y}_{\mathrm{B}}^{n_0}$ using the TMM method [27] for the n_0-th modal contribution. Due to the reduced dimension of the minimization problem and to keep the computational cost of this minimization procedure as low as possible, the Nelder-Mead Simplex Method has been used [28]. Consequently, since this fitting procedure is repeated in a frequency-by-frequency sweeping, the use of this kind of derivative-free optimization algorithms guarantee the overall efficiency of this methodology. Obviously, other optimization strategies could be used for this purpose, such as genetic algorithms [29] or efficient global optimization procedures [30].

As it has been highlighted in Remark 3.9, the inverse problem solved for the characterization of porous materials has infinity (but countable) solutions due to phase changes on the wave number values. Since, the primal unknowns $\delta_{\mathrm{P}}(\omega)$ and $\delta_{\mathrm{Q}}(\omega)$ drive the complex phase of $\beta_{\mathrm{P}}^{n_0}(\omega)$ and $\beta_{\mathrm{Q}}^{n_0}(\omega)$, respectively, the drawback of multiple solutions could lead to a discontinuous behavior with respect to the frequency of this unknowns in the solution of the minimization

problems (16) and (17). Consequently, to guarantee a continuous behavior of the primal unknowns with respect to the frequency, five simultaneous strategies have been utilized to complement the use of the Nelder-Mead method: (a) for a given set of angular frequency values, problems (16) and (17) are solved sequentially from the highest frequency to the lowest one; (b) the initial guess in the minimization method for the highest frequency have been computed (see Remark 5.1) by assuming that $\beta_{\mathrm{P}}^{n_0} \approx \beta_{\mathrm{F}}^{n_0} - 10j$ and $Z_{\mathrm{P}} \approx Z_{\mathrm{F}} - j\mathrm{Re}(1/Y_{\mathrm{I}})$ (analogous considerations are made for the initial guesses of quantities related to the second porous layer in Ω_{Q}); (c) the initial guess for subsequent frequencies are given by the solution of the previous solution for a higher frequency; (d) the low-frequency limit of the real part of the dynamic mass density is assumed known (in order to fix the value of the wave number phase at lowest frequencies), and (e) an unwrapping procedure is performed on the frequency dependent values of $\beta_{\mathrm{P}}(\omega)$ and $\beta_{\mathrm{Q}}(\omega)$ to avoid possible jump discontinuities. All these strategies have been used to obtain the numerical results presented in the following section.

Remark 5.1. *The initial guesses for the imaginary parts of the porous wave number and the porous characteristic impedance have been derived from the expression of the input impedance of a porous layer of thickness d backed by a rigid wall, this is,*

$$Z_{\mathrm{I}}(\omega) = Z_{\mathrm{P}}(\omega)/\tanh(j\beta_{\mathrm{P}}^{n_0}(\omega)d). \tag{18}$$

On one hand, assuming that the porous layer is highly absorbing at high frequencies, then $\mathrm{Im}(\beta_{\mathrm{P}}^{n_0}(\omega)) \ll 0$ *and so* $|\tanh(j\beta_{\mathrm{P}}^{n_0}(\omega)d))| \approx 1$. *Due to the exponential decreasing behavior of* tanh*, it is enough to assume* $\mathrm{Im}(\beta_{\mathrm{P}}^{n_0}(\omega)) \approx -10$ *to obtain* $|\tanh(j\beta_{\mathrm{P}}^{n_0}(\omega)d))| \approx 1$. *On the other hand, at the frequency range of the present work,* $\mathrm{Re}(\beta_{\mathrm{P}}^{n_0}(\omega)d) \gg \mathrm{Im}(\beta_{\mathrm{P}}^{n_0}(\omega)d)$. *Hence, neglecting the imaginary part of the wave number,* $\tanh(j\beta_{\mathrm{P}}^{n_0}(\omega)d)) \approx \tanh(j\mathrm{Re}(\beta_{\mathrm{P}}^{n_0}(\omega))d)$ *whose real part is null. So, Eq.* (18) *leads to* $Z_{\mathrm{I}} \approx jZ_{\mathrm{P}}|\tanh(j\mathrm{Re}(\beta_{\mathrm{P}}^{n_0}(\omega))d)| \approx jZ_{\mathrm{P}}$ *and hence the imaginary part of the porous characteristic impedance is estimated from the real part of the input impedance* $Z_{\mathrm{I}} = 1/Y_{\mathrm{I}}$.

6. Numerical results

In this section, the characterization results obtained with the proposed methodology will be analysed taking into account experimental measurements in single and double layer configurarions. Two different type of surface admittance experimental data are considered. These experimental data have been determined from measurements in an impedance tube (see Figure 4). Firstly, the surface admittance data is measured using the impedance tube for a single layer configuration. Second, the same measurements have been performed in the case of a double layer configuration. In both cases, it has been considered the frequency range in which the loudspeaker excites only the first transverse mode of the tube.

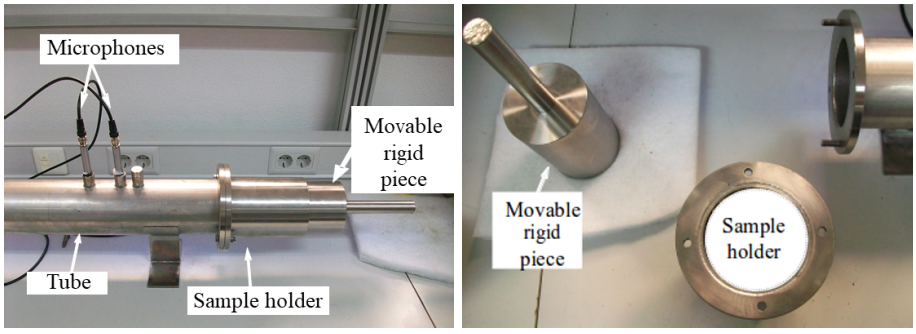

Figure 4: Impedance tube used to obtain the surface admittance the experimental data. On the left, it is shown the tube and the location of the microphones, along with the porous (multi)layer sample holder and the movable piece that serves as rigid termination. On the right, it is shown a detail of the movable rigid piece and the sample holder where the porous layers are placed.

Figure 5 shows the samples of porous materials used in the experimental measurements in both single and double layer configurations.

6.1. Single layer configuration

The experimental data used are the surface admittance of a setup with the single porous layer (see left picture in Figure 5) where the two datasets $Y_{\mathrm{I}}(\omega)$ and $\tilde{Y}_{\mathrm{I}}(\omega)$ involve respectively a rigid backing, this is, $Y_{\mathrm{B}}^{0} = 0$ and an air gap of thickness $s = 0.025\,\mathrm{m}$ between the porous layer and the rigid backing (so

Figure 5: Samples of porous materials used in the experimental measurements. Sample marked with number "1" is formed by a recycled foam, which has been used for the single layer configuration (left). Sample marked with number "4" is made by a fibrous material. Both samples have been used in the double layer configuration.

straightforward computations lead to $\tilde{Y}^0_{\mathrm{B}}(\omega) = Y_{\mathrm{F}}(\omega)/\tanh(j\beta^0_{\mathrm{F}}(\omega)s))$ following the two-cavity method [14].

The material measured in the impedance tube is a fibrous material with thickness $d = 0.03$ m. The experimental data used in the fitting problem (16) are the surface admittance of the setup with air gap and without air gap. Moreover, the real part of the dynamic mass density at low frequency has been set such that $\ell = 0$ in (12). The relative errors resulting from this fitting are around $10^{-6}\%$. Figure 6 shows the numerical values of different acoustic quantities, to list: characteristic impedance and wave number; computed by using the optimal values obtained with the fitting procedure. In these plots, they are compared with those values obtained with the Utsuno closed form expressions analogous to those ones given by (10)-(11).

The accurate agreement between the Utsuno closed-form expressions and the solution computed with the minimization procedure described in Section 5 confirms the robustness and accuracy of the proposed general approach for the analyzed case, where all the acoustic data is treated by an algorithm based on frequency-by-frequency computations.

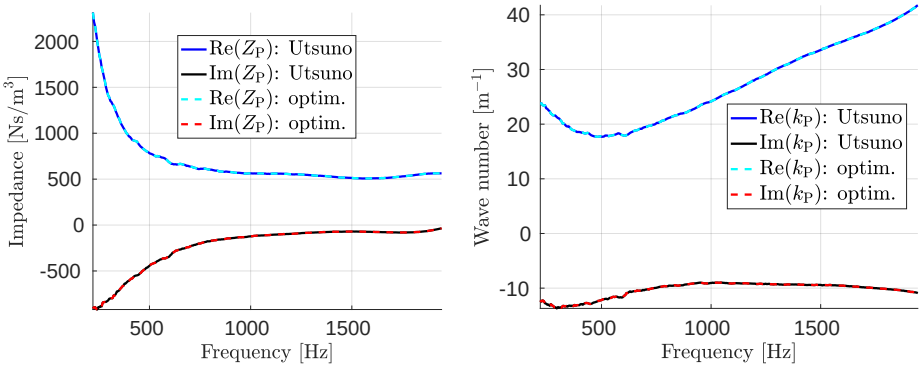

Figure 6: Comparison of the characteristic impedance (left) and the wave number (right) of the porous material in a single layer configuration computed by using the optimal values obtained in the fitting problem (16) and the Utsuno expressions (10)-(11).

6.2. Double layer configuration

The multilayer problem under consideration is formed by two porous layers with thickness $h = 0.045$ m and $d-h = 0.032$ m, respectively (the materials used in this case are a fibrous material and a recycled foam shown in Figure 5). Since the unknown parameters are the dynamic mass density and the wave number of the two layers, i.e., $\mathrm{Re}(\rho_{\mathrm{P}})$, $\mathrm{Im}(\rho_{\mathrm{P}})$, M_{P}, δ_{P} and $\mathrm{Re}(\rho_{\mathrm{Q}})$, $\mathrm{Im}(\rho_{\mathrm{Q}})$, M_{Q} and δ_{Q}, it is necessary to consider four surface admittance datasets for the solution of the minimization problem (17). Therefore, the experimental data used in the fitting problem are the surface admittance of each porous layer separately with rigid back admittance ($Y_{\mathrm{B}}^0 = 0$ and $\tilde{Y}_{\mathrm{B}}^0 = 0$ in the datasets i) and iii) of the inverse Problem 4.1) and additionally the surface admittance data of two different double multilayer configurations where the order of the porous layers have been inverted (datasets ii) and iv) of the inverse Problem 4.1). In both of them, the back admittance is assumed rigid, this is, $\hat{Y}_{\mathrm{B}}^0 = 0$ and $\breve{Y}_{\mathrm{B}}^0 = 0$. Once the minimization problem (17) has been solved using these four datasets, the frequency-dependent intrinsic coefficients can be identified.

Figure 7 shows the characteristic impedance $Z_{\mathrm{P}}(\omega)$ and the wave number $k_{\mathrm{P}}(\omega)$ of the porous material in the first layer. Analogously, Figure 8 shows the frequency-dependent responses for the acoustic quantities $Z_{\mathrm{Q}}(\omega)$ and $k_{\mathrm{Q}}(\omega)$,

which determines the acoustic behavior of the second layer. It can be observed that the responses of every acoustic quantity is continuous for middle and high frequency regime. Notice that Figures 7 and 8 show spurious oscillations at low frequencies due to the presence of errors in the experimental measurements of the surface admittance in the same frequency range (see those oscillations at low frequency regime in the data plotted in Figure 7).

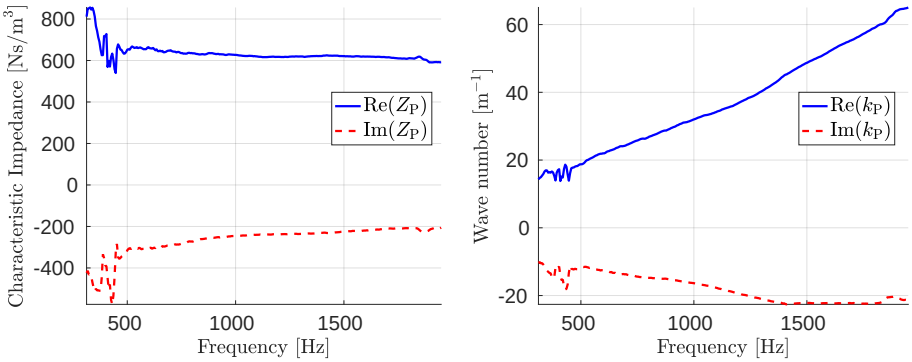

Figure 7: Real part (solid line) and imaginary part (dashed line) of the characteristic impedance $Z_P(\omega)$ (left) and wave number $k_P(\omega)$ (right) associated to the porous material located in the first layer computed from the solution of the minimization problem (17).

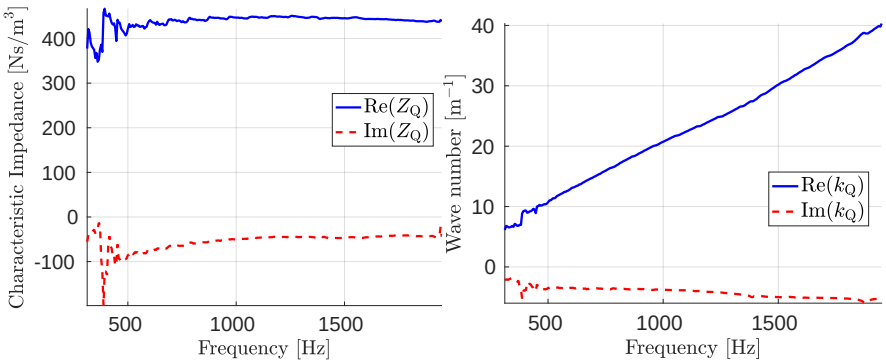

Figure 8: Real part (solid line) and imaginary part (dashed line) of the characteristic impedance $Z_Q(\omega)$ (left) and wave number $k_Q(\omega)$ (right) associated to the porous material located in the second layer computed from the solution of the minimization problem (17).

7. Conclusions

A non-parametric approach was has been proposed to predict the acoustical properties of porous materials with rigid solid frame. The adopted procedure is based on solving a sequence of frequency-by-frequency well-posed inverse problems, but without the requirement of using any theoretical parametric model. This approach makes use of the experimental data obtained using only a two-microphone impedance tube setup [13], thus avoiding the need for sophisticated laboratory equipment. The well-posedness of the inverse problem has been analyzed in detail showing that two surface admittance datasets with different backings is the only requirement to identify accurately the acoustic properties of a porous material in the case of single porous layer configurations. For double porous layer configurations, it has been shown that four surface admittance datasets are necessary to state a well-posed inverse problem. In both cases, the proposed methodology produces fitting relative errors smaller than $10^{-6}\%$. In addition, this method has been compared with the closed-form analytical expressions proposed by Utsuno *et al.* [14] for single layer configurations, showing a good agreement. In comparison, the proposed methodology not only avoids the assumptions made by the former, but also allows a wider applicability to single and multiple layer configurations. In this latter regard, the need for characterization procedures that let tackle with light porous layers is of great interest because of the associated technical difficulties in the experimental measurements, thus making this approach an interesting in the design stage of porous materials. In conclusion, the present work shows that the acoustic properties of porous materials can be accurately predicted by adopting this non-parametric methodology.

Acknowledgements

This work was also developed in the scope of COST (European Cooperation in Science and Technology) through the COST Action CA15125 - DENORMS: Designs for Noise Reducing Materials and Structures. The second author has

been partially supported by Xunta de Galicia project "Numerical simulation of high-frequency hydro-acoustic problems in coastal environments - SIMNUMAR" (EM2013/052), cofunded with European Regional Development Funds (ERDF) and by the Spanish Ministerio de Economía y Competitividad under project MTM2016-76497-R.

References

[1] K. Attenborough, K. M. Li, K. V. Horoshenkov, Predicting Outdoor Sound, Taylor & Francis, 2006.

[2] F. Fahy, Foundations of Engineering Acoustics, Academic Press, 2001.

[3] J. F. Allard, N. Atalla, Propagation of Sound in Porous Media: Modelling Sound Absorbing Materials, John Wiley & Sons, 2009.

[4] D. L. Johnson, J. Koplik, R. Dashen, Theory of dynamic permeability and tortuosity in fluid-saturated porous media, Journal of Fluid Mechanics 176 (1987) 379402.

[5] Y. Champoux, J. F. Allard, Dynamic tortuosity and bulk modulus in air-saturated porous media, Journal of Applied Physics 70 (1991) 1975–1979.

[6] M. A. Delany, E. N. Bazley, Acoustic properties of fibrous absorbent materials, Applied Acoustics 3 (1970) 105–116.

[7] T. J. Cox, P. D'Antonio, Acoustic Absorbers and Diffusers: Theory, Design and Application, Taylor & Francis, 2009.

[8] J. A. Nelder, R. Mead, A simplex method for function minimization, The Computer Journal 7 (4) (1965) 308–313.

[9] P. Bonfiglio, F. Pompoli, Inversion problems for determining physical parameters of porous materials: Overview and comparison between different methods, Acta Acustica united with Acustica 99 (2013) 341–351.

[10] M. Vasina, D. C. Hughes, K. V. Horoshenkov, L. Lapčík Jr., The acoustical properties of consolidated expanded clay granulates, Applied Acoustics 67 (2006) 787–796.

[11] A. Geslain, J. P. Groby, O. Dazel, S. Mahasaranon, K. V. Horoshenkov, A. Khan, An application of the peano series expansion to predict sound propagation in materials with continuous pore stratification, Journal of the Acoustical Society of America 132 (1) (2012) 208–215.

[12] K. Attenborough, Acoustical characteristics of porous materials, Physics Reports 82 (3) (1982) 179–227.

[13] I. 10534-2, Acoustics–Determination of sound absorption coefficient and impedance in impedance tubes–Part 2: Transfer-function method, Tech. rep., ISO (1998).

[14] H. Utsuno, T. Tanaka, T. Fujikawa, A. F. Seybert, Transfer function method for measuring characteristic impedance and propagation constant of porous materials, Journal of the Acoustical Society of America 86 (2) (1989) 637643.

[15] B. H. Song, J. S. Bolton, A transfer-matrix approach for estimating the characteristic impedance and wave numbers of limp and rigid porous materials, Journal of the Acoustical Society of America 107 (3) (2000) 11311152.

[16] O. Doutres, Y. Salissou, N. . Atalla, R. Panneton, Evaluation of the acoustic and non-acoustic properties of sound absorbing materials using a three-microphone impedance tube, Journal of the Acoustical Society of America 71 (6) (2010) 506–509.

[17] X. Xiong, W. Shi, Y. Hon, A one-dimensional inverse problem in composite materials: Regularization and error estimates, Applied Mathematical Modelling 39 (18) (2015) 5480 – 5494.

[18] R. Keshavarz, A. Ohadi, A new analytical approach for the modeling of sound propagation in a stratified medium, Applied Mathematical Modelling 50 (2017) 237 – 256.

[19] Mahmood-ul-Hassan, Wave scattering by softhard three spaced waveguide, Applied Mathematical Modelling 38 (17) (2014) 4528 – 4537.

[20] R. E. Collin, Field Theory of Guided Waves, IEEE Press, 1991.

[21] D. Givoli, Numerical Methods for Problems in Infinite Domains, Vol. 33, Elsevier, 2013.

[22] F. Ihlenburg, Finite Element Analysis of Acoustic Scattering, Vol. 132, Springer, 2006.

[23] Y. Salissou, R. Panneton, O. Doutres, Complement to standard method for measuring normal incidence sound transmission loss with three microphones, Journal of the Acoustical Society of America 131 (3) (2012) EL216EL222.

[24] R. Panneton, Comments on the limp frame equivalent fluid model for porous media, The Journal of the Acoustical Society of America 122 (6) (2007) EL217–EL222.

[25] D. R. Smart, Fixed Point Theorems, Vol. 66, Cambridge University Press, 1980.

[26] J. Carbajo, A. Prieto, J. Ramis, L. Río-Martín, Data-driven characterization of porous materials by using frequency-dependent measurements, in: Tecniacústica 2017: 48º Congreso Español de Acústica; Encuentro Ibérico de Acústica; European Symposium on Underwater Acoustics Applications; European Symposium on Sustainable Building Acoustics: A Coruña 3-6 Octubre 2017, Sociedad Española de Acústica, 2017, pp. 739–746.

[27] L. M. Brekhovskikh, Waves In Layered Media, 2nd Edition, Applied Mathematics and Mechanics, Academic Press, 1980.

[28] J. C. Lagarias, J. A. Reeds, M. H. Wright, P. E. Wright, Convergence properties of the Nelder–Mead simplex method in low dimensions, SIAM Journal on Optimization 9 (1) (1998) 112–147.

[29] V. Romero-García, E. Fuster-Garcia, J. Sánchez-Pérez, L. Garcia-Raffi, X. Blasco, J. Herrero, J. Sanchis, Genetic algorithm in the optimization of the acoustic attenuation systems, in: International Work-Conference on Artificial Neural Networks, Springer, 2007, pp. 614–621.

[30] R. Morgans, C. Howard, A. Zander, C. Hansen, D. Murphy, Derivative free optimisation in engineering acoustics, in: ICSV14: Proceedings of the 14th International Congress on Sound and Vibration, AAS, 2007, p. Paper 126.